System and Methods for Hybrid Lunar Surface and Space Domain Situational Awareness

Elvis D. Silva, Jeffrey Van Cleve, Rob Philbrick,
Christopher J. Grant, Jacob D. Griesbach, Michael P. Mahoney
Ball Aerospace

ABSTRACT

Supporting cislunar space and lunar surface domain awareness has typically required the design and use of intrinsically distinct payloads with different operation modes and techniques: one for detection and tracking of very dim moving point sources against the background of space, another for surface imaging and processing (lunar surface intelligence, or surface monitoring). Here we present a representative single sensor design achieved by using an electro-optic (EO) signal chain that is capable of a hybrid function. First, the single sensor design looks to balance performance to enable a 2m GSD during moon surface observation periods while maximizing SNR performance to the libration points L1 and L2 for space situational awareness missions. Next, the single sensor design is evaluated against a variety of orbital configurations to examine combined (sensor/orbit) performance against lunar surface metrics, as well as space domain awareness in the near moon space. The reference architectures are evaluated under various lighting conditions.

1. INTRODUCTION

As we continue to transition from Space Situational Awareness (SSA) to Space Domain Awareness (SDA), the cislunar space domain is the next frontier. The expansion of use of the cislunar space domain by space fairing nations as well as private business interests has driven growth in traffic transiting the cislunar domain as well as activity on the lunar surface. Scientific and space mining missions to the moon are hot discussion topics today, which implies that future missions to cislunar space will become more plentiful. As this commercial and scientific interest continues to grow, the ability to monitor and manage these activities also increases. NASA and the U.S Space Force have already established a foundation of broad collaboration to meet these goals through a new Memorandum of Understanding 1. With this, the community must be ready to surveil, track, and assess remote space objects (RSOs) in this new space to perform space traffic management (STM) to provide safe manned and freight transit in this new regime. In addition, there is continued scientific and strategic interest to perform monitoring of the lunar surface. Surface awareness can aid the identification of future landing sites, activity monitoring, etc.

Over the last year, there has been substantial new activity and research conducted regarding cislunar SDA. The 2020 AMOS Conference included space policy discussions regarding cislunar space and several technical presentations on sensor solutions to address the regime 2. John Hopkins University /Applied Physics Laboratory has established a new Cislunar Security Conference. AFRL/RV is conducting two studies exploring near-lunar SDA (CHPS) and cislunar logistics (ADOX). Academia and industry have also partnered to familiarize the industry with how to answer the call to develop plans, capabilities, expertise, and operational concepts for cislunar space 3. All of these forums include architectural recommendations for potential future consideration. Depending on the type of mission domain (cislunar SDA or surface monitoring), careful selection of adequate orbits plays a role in the lighting, geometric, and access conditions to each domain. The novel system proposed herein uses a modern imaging CMOS FPA sensor with a hybrid (framing + TDI) capability to define a single telescope design in combination with orbit configuration to perform Lunar surface and Lunar space domain awareness missions.

2. SENSOR DESIGN / BACKGROUND

The cislunar application described herein requires both staring and Time Delay and Integrate (TDI) sensor operation to accomplish the mission. A two-sensor solution – e.g., an 8k column x 2k row CMOS staring sensor plus an 8k x 32 row CMOS TDI sensor – could be combined in a single telescope design. Such a solution requires two sets of command-and-control electronics – one for each CMOS sensor – and results in significantly higher instrument size, weight, and power (SWaP). We focus on CMOS-based sensors, as opposed to CCD-based sensors, because we expect this to be a multiple year mission in lunar space environment. An alternative FPA solution is to deploy a single 8k x 2k staring sensor and operate it in window readout mode when used for scanning operation. In this mode, the time-

shifting and aggregation functions associated with TDI operation are all performed off sensor in a support FPGA. One shortcoming of this off-chip TDI solution is the entire TDI area, in this example 8k cols x 32 rows, still needs to be digitized and read off the sensor each frame (scan line). This, in turn, limits the maximum effective scanning line rate the sensor can support. Continuing the above sensor example, and assuming on-chip ADC resolution is 14 bits/pixel and the maximum desired serial rate is 2 Gbps per output, the 8k x 32 row off-chip TDI solution would be limited to a maximum effective line scan rate of 545 lines per second (lps). The novel sensor solution described here – with on-chip TDI functionality for 32 rows – supports a maximum scan rate of 12k lps, assuming the on-chip TDI memory is now 20 bits deep. Adding outputs to either sensor solution increases the maximum scan rate proportionally.

The sensor solution we propose is illustrated in Fig. 1, where the active area is 8192 columns (C1) by 2048 rows (R1). The first 32 (R2) rows of the active area are mapped into on-chip circuitry that performances the TDI time shifting and aggregation functions (on-chip). While operating in TDI mode, each frame (line) period only 8192 col x 1 row x 20 bits of data is output. (The higher memory depth of 20 bits is needed to accommodate the summation of 32, 14 bit samples.) The sensor design supports bidirectional TDI scanning and programmable TDI rows between 1 and R2. Using the calculation described above, this sensor supports TDI scanning speeds of 12k, 24k, 36k, and 48k lps if the sensor uses 1, 2, 3, or 4 outputs, respectively. This sensor solution performs both the staring and scanning functions needed by the cislunar mission using a single telescope and focal plane, thereby minimizing instrument SWaP.

Being a CMOS-based sensor, the TDI aggregation occurs in the digital domain. Therefore, unlike in CCD-based sensors which perform noiseless TDI summation in the charge domain, the TDI summation step adds noise and signal with each pixel sample. The net improvement in signal to noise ratio while operating in TDI mode is sqrt(R2), or in the above example a factor of 5.7. As with all scanning applications, the scanning speed must be properly balanced with the telescope radiometric throughput. This CMOS sensor has the added feature of programmable integration time per frame, whether in TDI or staring mode. Therefore, extremely bright scenes can be handled without changing the line rate by simply programming the per frame integration period to a lower setting. During normal staring (a.k.a. full frame) imaging, all C1 x R1 rows of image data are output, thereby maintaining the full field of view. The sensor supports both rolling and global shutter staring modes of operation.

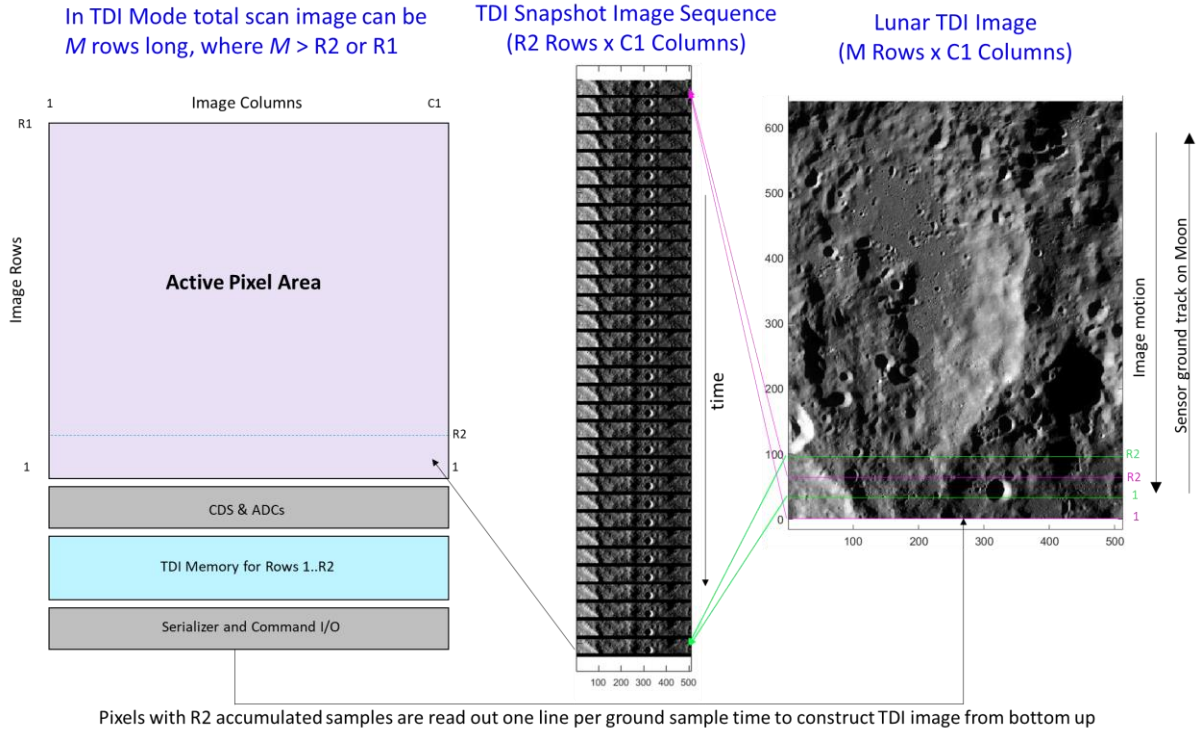

Fig. 1. Block diagram of novel CMOS image sensor that supports staring and on-chip TDI functionality (left), example of integrated image collects from TDI region (in TDI mode, center), and representation of how full frame images are shifted and summed in TDI memory to create a scanned image (right).

3. TELESCOPE DESIGN

Telescope design is tightly coupled to mission design, an obvious example being the relationship between target flux, FOV, FOR, IFOV, revisit time, and required SNR. This paper is unique in that the same telescope must serve two distinct target domains: deep space for SDA, and the lunar surface for surface monitoring. Some qualitative apportionment of merit to SDA and surface monitoring then guides a compromise between a system optimized for SDA and one optimized for surface monitoring, as noted in Section 2. In this paper, we'll consider a system that spends most of its time searching space near the Moon, and a small fraction of its time looking at the lunar surface, either targeting sites of known activity, or looking for changes over some portion of the lunar surface. This weighting is guided by the notion that, at least through 2030, anthropogenic activity on the lunar surface will be confined to a relatively small area near the lunar poles, or a small number of landing sites in other regions.

Design considerations for the SDA mission include telescope pupil area A ($\pi D^2/4$) and the solid angle Ω of the FOV. Typically, large telescopes have small Ω and small telescopes can have larger Ω, with AΩ or 'etendue' being an informal measure of optical difficulty. For efficient observing, the telescope must also spend most of its time collecting photons instead of slewing and settling. Since moments of inertia scale as the fifth power of linear dimension, big telescopes are hard to move quickly and typically cost more as roughly D^2. The optimal design is typically a compromise between a telescope that's too small to cover the FOR in the revisit time and one that's too big to be efficient in cost or observing time. The SDA mission also pushes in the direction of larger IFOVs, since a given number of pixels can cover more of the sky if the IFOV is bigger.

Design considerations for surface monitoring include the GSD and the illumination levels of the lunar surface, which push the design towards smaller IFOVs for better GSD at a given altitude, and very short integration times, on the order of the GSD at nadir periapse divided by velocity. surface monitoring also benefits from arranging the pixels in a rectangle instead of a square, with the long axis cross-track, for a wider swath width projected on the lunar surface for search operations while maintaining the same Ω on the sky for SDA. This reformatting is limited when the effective F/# of the cross-track image become optically difficult, where the effective F/# combines the F/# of a point source and the angular width of the FOV in the cross-track direction.

For the SDA mission, we require SNR >= 6 on the benchmark SDA target at 90-degree phase angle at a range equal to the geometric mean of the ellipsoid axes shown in Fig. 2 = 55,000 km. The benchmark target thus has $m_v = 16.9$. We also need to achieve this SNR while sweeping the sky at 1.0 square degrees/s, which may be thought of as covering 4π in half a day, much shorter than timescale of motion within Lagrangia or of the time spent transiting Lagrangia on and Earth-Moon trajectories.

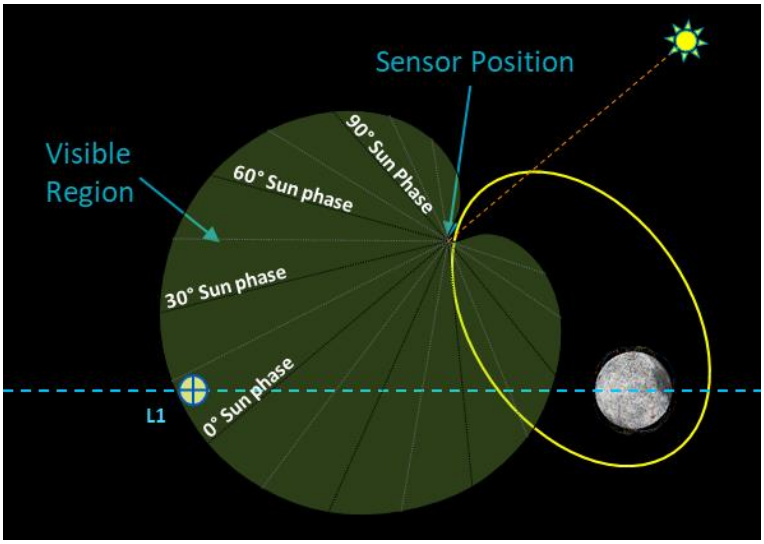

Fig. 2. Lunar search volume covers the space from 10,000 km beyond L1 to 10,000 km beyond L2 and a width of 30,000 km near the moon.

For surface monitoring, GSD <= 0.5 m at periapse. GSD requirements are determined by examination of Apollo 15 images in the LRO NAC dataset at resolutions of 0.5, 1.0, and 2.0 m/pix and by the science requirement of being able to see fresh ~1.0 m craters 45. Of course, lower altitudes have small GSDs for a given IFOV, but we will bound the problem by setting a minimum altitude of 30 km for orbital stability based on LRO orbit maintenance 6. The per-pixel SNR must be > 20 for solar elevation of 1.5 degrees, 10% albedo surface to image locally flat regions at the poles at solstice. It is also desired, but not initially required, that the surface monitoring swaths must overlap within 2.5° of periapse to cover the region of expected human activity near the S. Pole if periapse

is targeted for the S. Pole. Instrument design space has many dimensions so we will make a few assumptions to make the process tractable for this paper. First the wavelength range is panchromatic VIS, 400-900 nm to maximize SNR for objects reflecting sunlight. Second, the pixel pitch is 10 microns, read noise is 50 e-, and dark current is negligible, much like the Teledyne GeoSnap-10 we work with at Ball.

A strawman concept that meets these first-order requirements has a 30 cm aperture, a FOV of 6.0 x 1.5 degrees with the short axis along-track, an IFOV of 2.64" or 12.78 urad, and a 16 Mpix focal plane with 8 k pixels cross-track and 2 k pixels along-track. The effective F/# is 2.05 and the focal length is 78.2 cm. The optics are compact (hence low moment of inertia) with a reflective primary and secondary, and a series of refractive lenses to bring the image to final focus. For SDA, the telescope collects 5 x 1.2 s frames (5 frames for cosmic ray rejection) at each point on the sky, then slews and settles in 3.0 s. For surface monitoring, the SNR at 1.5-degree solar elevation is 40, using 8 TDI stages and a line rate of 4.0 kHz for a low circular orbit. The GSD is 0.50 m at 39 km altitude, while the swath width is 4.1 km. Imaging inside the PSRs, using scattered light from crater rims, could be possible if read noise could be reduced to 25 e- or less. Some focal planes have high and low gain outputs, in which low gain could be use in sunlit regions while high gain, with effectively lower read noise, would be used for imaging PSRs.

It is very important to note that these first-order parameters are not sufficient for good operational performance; not all 30 cm telescopes are alike, quality as well as size matters!

- To achieve the SNR and GSD, SDA pointing stability – the integral of jitter and drift over a frame time -- must be smaller than 0.5 pixels during a frame, or 1.32" 1-σ single-axis over 1.2s, well within the performance of our astronomical observatories.
- The telescope must be agile, so that the time spent slewing and settling is small compared to the amount of time collecting photons.
- The surface monitoring line rate must be matched to the projected surface velocity at each point on the orbit and focus adjusted between surface monitoring and SDA observations, as routinely done for the Ball-built HiRISE camera which has been operating in orbit around Mars for the last 15 years.
- The telescope focus must be adjusted between SDA and surface monitoring observations, as was also done for HiRISE when switching between stellar calibrators and the Martian surface.
- Excellent straylight control is required to observe objects close to the lunar limb. The methods shown the companion paper (Van Cleve+, 2021) for reasonably well-baffled telescope, when applied to platforms orbiting the Moon, gives a lunar limb avoidance angle of 15 degrees for a for straylight $m_v = 14.0$ per pixels. This limb avoidance angle defines the solid angle available for SDA at a given point in the orbit. Various methods, outside the scope of this paper, can be applied to reduce this angle.
- Likewise, baffle design must support a sun exclusion angle of 30 degrees without thermal distortion of the telescope or scattering onto the focal plane by single or multiple bounces. 30 degrees is a compromise between loss of sky access (6.7%) and design difficulty (baffle length, paint blackness, solar heat conductance, etc.)

4. MISSION DESIGN CONSIDERATIONS

The benefit of the Ball hybrid sensor design is the ability to address cislunar SSA and lunar surface monitoring missions with a single sensor. Flexibility in the sensor design allows for task-ability of the instrument depending on mission need as well as mission constraints such as surface lighting, deep-space lighting, orbit geometry relative to lunar surface as well as geometry relative to monthly variations to lighting and earth access. Although the sensor design provides flexibility to perform a variety of these missions, the architecture designer is posed with a set of design options to address their mission as it relates to either space or surface looking needs. With maneuverable spacecraft, the mission designer is further enabled to tailor orbital parameters to transition mission utility throughout the lifecycle of the spacecraft – for example, the designer could select a highly eccentric initial orbit heavily biased for more lunar surface access and transition the mission into a more SDA-specific mission by performing periapsis increase maneuvers and vise-versa.

In general, higher eccentricity orbits can provide longer SDA periods with slower-moving dynamics, smaller moon blockages, and less limiting lighting conditions, but have the drawback of providing lower lunar surface access periods. Conversely, LLOs provide longer periods of access to the lunar surface, and although LLOs can be used for

deep space SDA, they are limited by lighting, geometric and stray-light moon blockages, timing constraints, and high dynamic rates. Fig. 3 captures some of the trade-off between the balance of high-eccentricity high-apoapsis orbits vs LLOs.

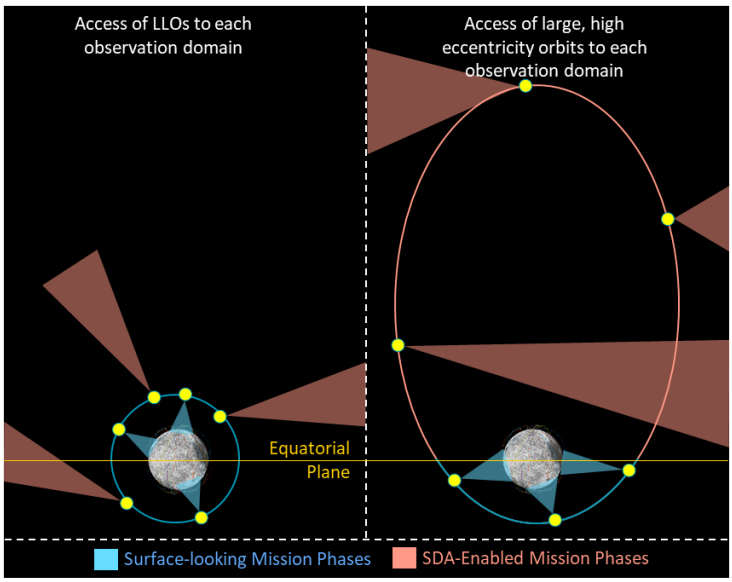

Fig. 3. Low-altitude orbits support longer periods of surface monitoring, high-eccentricity orbits can be used to balance SDA vs surface monitoring phases of a mission

Observing objects around cislunar space is heavily dominated by selected moon-orbiting parameters as well as monthly lighting conditions throughout the cislunar search volume. Ball's high-fidelity Visual Sensor Model (VSM) is used to assess detection range with respect to sun lighting conditions and stray light constraints. The VSM model is used to establish performance of the proposed sensor under various design conditions, including FPA details, specular lighting, jitter, smear, stray light, and celestial/galactic background effects. Simplistically, to first order, a sensor's performance can be depicted by a "cardioid" as depicted in Fig. 2. The cardioid represents detection range at various sun-phase angles for a target of specific size and albedo. The detection cardioid rotates in phase with the sun in the earth-moon rotating coordinate system. In general, for SDA-focused missions, orbits that create distance between the spacecraft and the earth-moon plane will benefit from favorable lighting conditions to access more space around the moon and depending on time of the month, the L1/ L2 locations (See case 1, NRHO orbits in Fig. 4). Alternatively, on the other extreme, the mission designer has flexibility to select circular Low Lunar Orbits (LLO) around the moon to increase moon-surface access at the cost of more restricted access to cislunar space, including the L1 / L2 locations (see Case 6, LLO in Fig. 4).

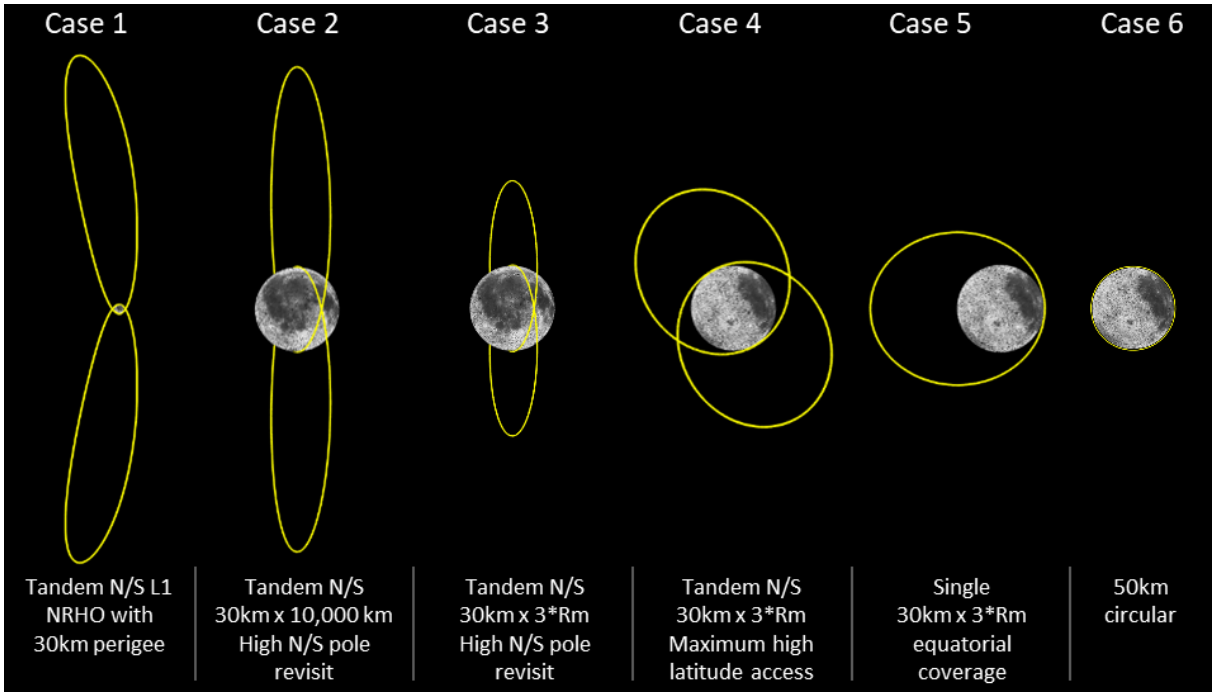

Fig. 4. Variation of orbit sizes, eccentricity, and periapsis placements create diverse observing geometries.

On the lunar surface, lighting conditions is dictated primarily by the solar day, or roughly a 29.5-day cycle. At higher latitudes, or near the poles, lighting conditions will be dictated by the lunar precession cycle, moon polar geometry relative to the ecliptic plane (time of year), and topography. Depending on the needs of the mission, lighting variation at the northern and southern poles creates conditions that the mission designer should consider when selecting orbits and will require more careful consideration of lighting in mission design 7. Beyond lighting conditions, the designer will also need to consider how to balance of access to the lunar surface (i.e., low altitude access to lunar surface) vs access to unconstrained deep space (i.e., high altitude apoapse into favorable lighting). In general, the hybrid sensor will be limited to a relatively narrow FOV resulting from the balancing of the SDA and surface-monitoring missions. In our configuration, we've selected an FPA tiling configuration that enables a 6° cross- track FOV for surface monitoring, the range at which this FOV provides a sub-2m GSD is below ~150km, and the range at which this provides a sub-10m GSD is below ~800km.

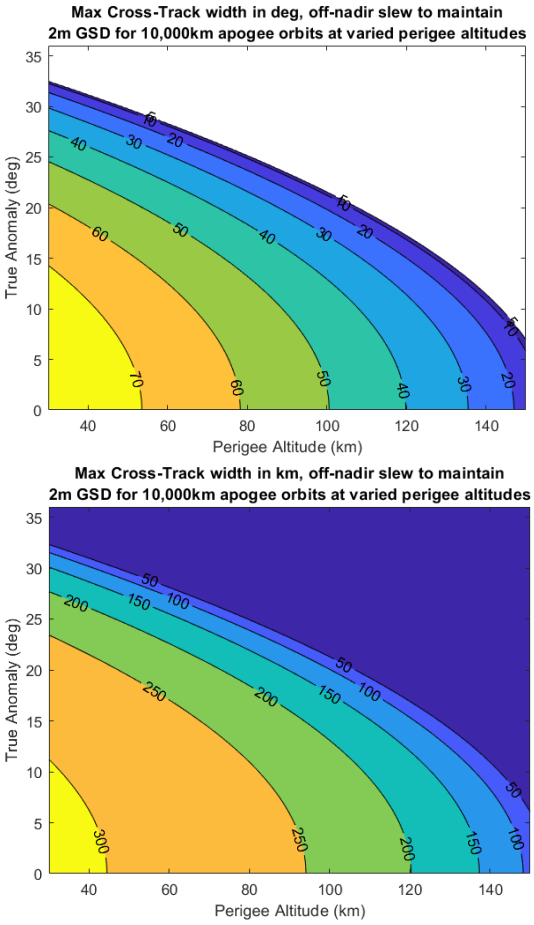

Fig. 5. Top: Half angle off-nadir slews needed to maintain 2m GSD. Bottom: Cross track width of access area at various periapsis altitudes and true anomalies.

In our analysis, we select extremely low-altitude periapses to enable access of lunar surface locations via off-nadir slews. At 30km perigee, large, off-nadir, cross-track slews of up to 80° can still access surface sites with a sub-2m GSD (shown at top of Fig. 5). This capability provides flexibility for the mission designer to enable access and revisit rates of various surface locations, at the cost of image distortion for large off-nadir slews. Fig. 5 shows max off-nadir, cross-track slews for families of periapses at varying true anomalies. An interesting family of orbits that can access low altitudes at predictable earth-moon geometry intervals are families of North/South L1/L2 NRHO orbits 8. The NRHO family of orbits have favorable, repeating access conditions for deep space cislunar SDA. At their apogee, the NRHO families can attain favorable lighting conditions and communication geometries at any point in the lunar month. Although the NRHO have favorable, repeating characteristics, their access to lunar

Table 1. Candidate orbit configurations create diversity in lunar surface and SDA viewing geometries.

		Case 1	Case 2	Case 3	Case 4	Case 5	Case 6
		NRHO Tandem	High apoapsis N/S Tandem	3R_M N/S Tandem	3R_M N/S Lat Coverage	3RM Equator Coverage	50km Circular Low Lunar
Orbit 1	Description	North L1 NRHO	North Polar	North Polar	North Polar	HEO Moon	LLO polar
	Periapsis (km)/Apoapsis (km)		30 / 10,000	30 / 3*R_M			50 / 50
	Inclination (deg)		90°				
	Argument of Periapsis (deg)		270°		305°	0°	
	Right-Ascension (deg)		0°				
Orbit 2	Description	South L1 NRHO	South Polar			None	None
	Periapsis (km)/Apoapsis (km)		30 / 10,000	30 / 3*RM			
	Inclination (deg)		90°				
	Argument of Periapsis (deg)		90°		125°		
	Right-Ascension (deg)		0°				
Orbit 1/2 Phasing			180°			n/a	n/a
Simulation Duration		Lunar Day					

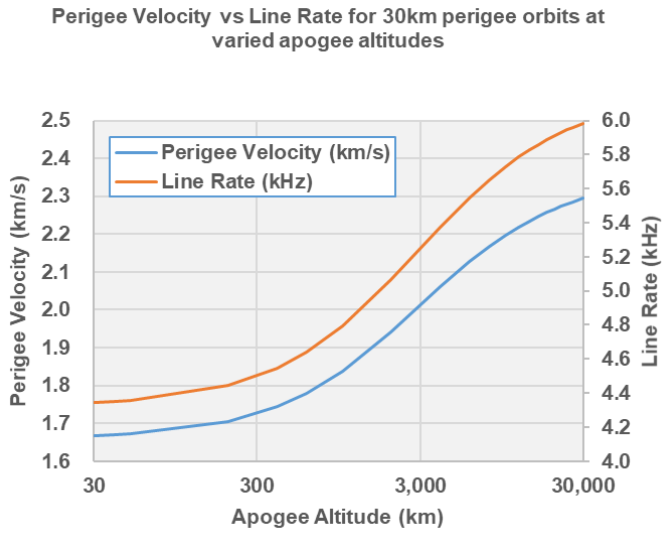

Fig. 6. Periapsis velocities (km/s) and line rates (kHz) for various 30km periapsis orbits and apoapsis varied to 30,000 km.

surface is limited to a subset of locations near the poles, and are therefore desirable for monitoring locations near the lunar poles.

Although surface mapping missions can be designed using the hybrid sensor, the small FOV characteristic of the design is a limiting factor for such missions; even for LLOs, mapping the entire moon surface requires long periods of time. While mapping missions are possible, the sensor's better utility is to monitor specific lunar sites. Selection of site monitoring orbits leverage orbit inclination and argument of periapsis to "center" the orbit's periapsis near the target of interest, while semimajor axis and eccentricity need to be "tuned" to balance latitude range to monitor, resolution during those access periods, and revisit rate or repeatability of ground-tracks. Flexibility in modifying orbit parameters (i.e., dv maneuverability) enables mission priorities (SDA vs surface-looking) as well as periapsis placement above the lunar surface to observe various locations around the moon (periapsis increase/lowering to target latitude/longitude locations).

Beyond GSD or ground resolution, periapse altitudes will also affect the operation of the focal plane array in TDI mode. Selection of orbits with higher apoapse will require operation of the TDI mode at fast enough line rates to match surface velocities at periapse. The selected FPA tiling configures a row of 8K pixels limited to just under approximately 1.76 Gbps, or a line rate of just under 12kHz for 19bit pixels. Circular 50km altitude orbits require line rates around 2.6 kHz, while high eccentricity orbits consisting of 30km periapsis with 30,000 km apoapsis will require line rates of just under 6kHz. Fig. 6 shows Periapsis velocities (km/s) and line rates (kHz) for orbit geometries with periapsis at 30km and apoapsis varied from 30km to 30,000 km.

In general, trajectories in the vicinity of the moon are dynamically limited to the space between L1 and L2, as a result, for purposes of this discussion, we define an ellipsoidal volume extending 10,000 km beyond L2 (~75,000 km in either L1/L2 direction) as shown in Fig. 7. The volume in Fig. 7 is representative of a volume of interest for most lunar space domain awareness missions. The cislunar volume covers L1/L2-centric trajectories such as halo 9 or Lissajous orbits as well as objects entering/exiting the volume via the L1/L2 points. The cross-section dimension of the ellipsoid is a radius of 30,000km to capture large DRO or NRHO family of orbits as well as highly eccentric moon trajectories. In addition to access in terms of volume coverage, we consider access to L1 and L2 as other metrics of interest. Further, per our optical design, we selected the SDA aspect of the sensors utility to be a primary mission focus, while moon-surface monitoring capabilities of this mission serve as a second tier focus of our hypothetical mission.

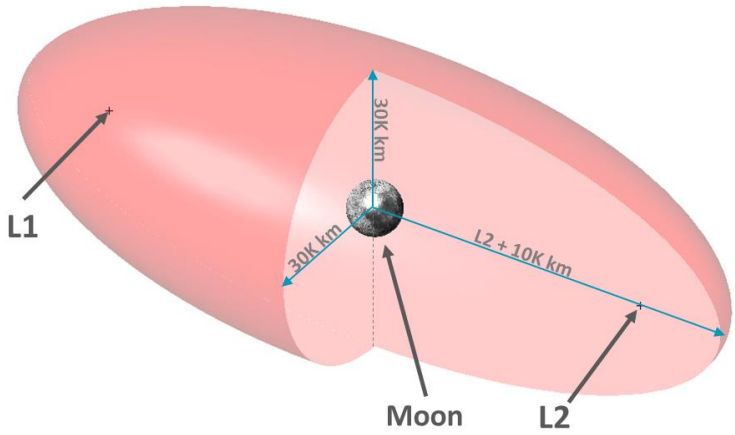

Fig. 7. Lunar volume of interest covers the space 10,000 km beyond L2 and L1 and covers a cross-section width of 30,000km from the moon.

Modeling Assumptions and Constraints

Our assessment of orbit configurations is representative but not exhaustive of options that a mission designer would evaluate with the hybrid sensor. Table 1 captures orbit configurations with variations in apoapsis altitudes, periapsis rotations, and eccentricity variations to exemplify surface monitoring configurations as well as deep-space monitoring configurations. Case one represents tandem N/S L1 NRHO orbits with 30km periapsis passes, this configuration is intended to represent a more SDA-focused mission; large spans of time spent performing SDA mission in deep cislunar space and limited time monitoring the lunar surface. Case two through four are tandem symmetric polar orbits with variation on apoapsis altitudes and argument of periapsis clocking; case two and three capture shorter range of latitudes at two of the moon's hemispheres. Case 3 orbit 1 precession in the moon-fixed frame is shown at left on Fig. 8. Case four captures a larger range of latitudes but only on one of the moon's hemispheres at a time. Case 5 is a single orbit configuration and covers a range of latitudes centered at the equator with a precessing longitude in the moon-fixed frame, shown at right side of Fig. 8. Case 6 is a 50km LLO with unrestricted access to the lunar surface and more restricted access to deep space for SDA.

To assess the characteristics of each selected orbit against the established space domain and surface monitoring aspects of missions, orbits were selected to encompass large variation in geometries, orbital periods, and altitudes relative to the lunar surface. The purpose of this assessment is not to establish a detailed assessment of performance under all sources of error or perturbations, but rather, to establish a rough understanding of the characteristic access metrics related to the selected orbits and understand how their implications on design trades. To this end, we've made the following assumptions to simplify our analysis:

- Except for the NRHO orbits (case 1), orbit propagation is based on a Keplerian model centered at the moon. This approach is used to avoid orbit parameter evolution because of external forces, and to circumvent the need to include station-keeping maneuvers in our simulation.
- Geometric and shadowing effects of the moon on cislunar volume are included in our access analysis, as shown in Fig. 9.
- A limb stay-out of 15° from the moon limb (lit or unlit), as shown in Fig. 9, is included in our access calculations. More advanced models may include moon lighting effects to increase access to volumes just over the moon.
- Our experience indicates that including a 30° sun stay-out cone, as shown in Fig. 9, is also important to reduce stray-light effects and damage to the sensor components. This constraint is included in our simulation.
- Baseline target has an Mv = 16.9, which represents at SNR6, 1m diameter target at 55,000km and 90° phase
- SDA observations are assumed to only be constrained by the parameters above, further, we incorporate the ability to observe targets during periapse passes in our simulation.

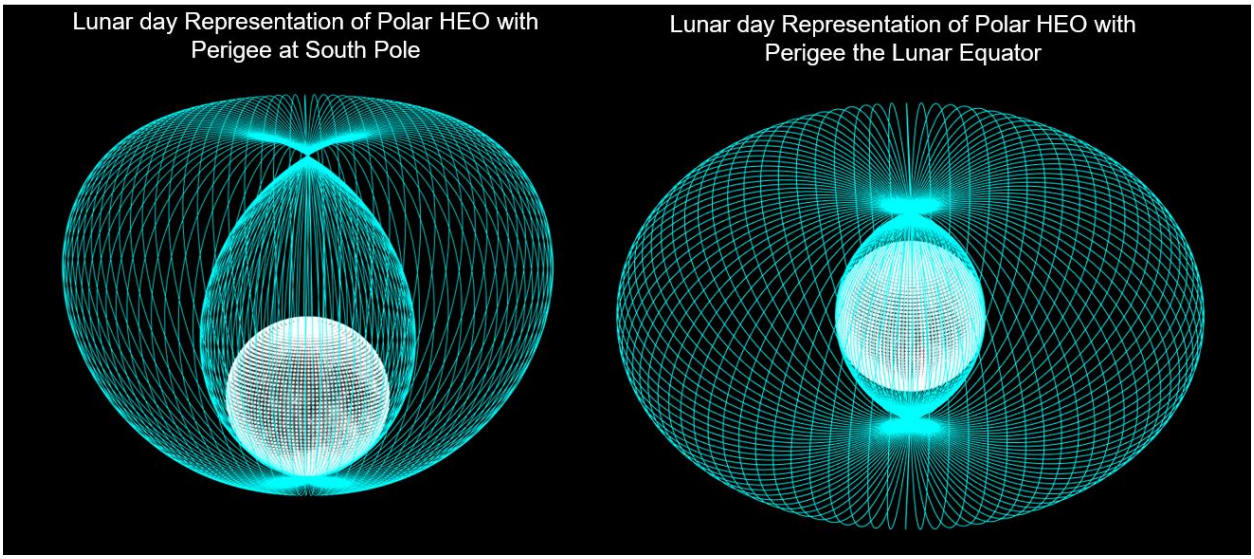

Fig. 8. Placement of periapsis relative to lunar surface provides access to range of longitudes over a lunar day.

- Surface monitoring observations are only gathered at altitudes and slew angles where sub-2m GSD is possible. Our analysis assesses field of regard and assumes the sensor's FOV can be placed within the desired location in the field of regard.
- No assumptions are made on spacecraft agility, attitude control, or other platform design concepts

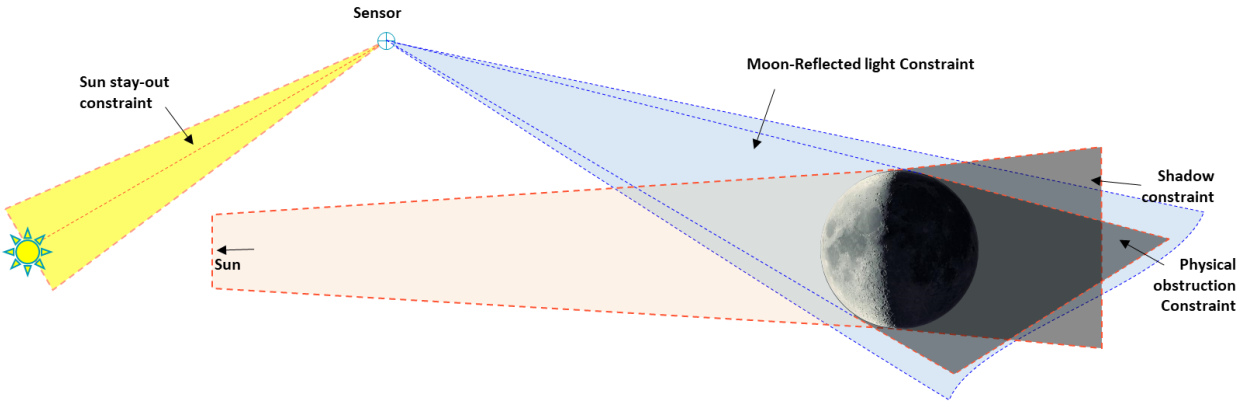

Fig. 9. Geometric, obstruction, lighting, and sensor performance constraints included in our simplified assessment of sensor performance in SDA domain. This drawing is not to scale.

5. Insights into Sensor Performance in Selected Architectures

General characteristics relating to altitude ranges, orbit periods, individual and combined/tandem access to SDA and lunar surface, earth access and periods of time in sun illumination are presented in Table 2 for each of the cases established in Table 1 and Fig. 4. The goal of this assessment is to characterize our understanding of access times the mission designer would expect to spend performing lunar surface monitoring vs deep space SDA, as well as a combined system (tandem) performance in each of these observation regimes. At 30km periapse altitude, the high-eccentricity orbits spend between 13 to 18 minutes within access to sub-2m GSD imaging opportunities. Based on our FPA format, these equate to 600-900Gb of data per periapse pass.

Table 2. General characteristics and performance profiles of selected architectures.

Generic results	Case 1	Case 2	Case 3	Case 4	Case 5	Case 6
Min Distance to moon surface (km)	30	30	30	30	30	50
Max Distance to moon surface (km)	~96,600	10000.0	3*Rm	3*Rm	3*Rm	50.0
Orbit Period (min)	12051	829	430	430	430	114
Orbit Period (hrs)	200.8	13.8	7.2	7.2	7.2	1.9
Time in SSA per orbit (min)	12037.8	813.4	411.9	411.9	411.9	113.8
Time in SSA per orbit (hrs)	200.6	13.6	6.9	6.9	6.9	1.9
% of Orbit spent in SSA	100%	100%	100%	100%	100%	100%
Time in surface monitoring per orbit (min)	13.1	16.0	17.8	17.8	17.8	113.8
Orbit percent spent in surface monitoring (%)	0.11%	1.9%	4.1%	4.1%	4.1%	100.0%
surface monitoring true anomaly range (deg)	±30.0°	±32.6°	±34.8°	±34.8°	±34.8°	±180°
Tb Generated during each pass	1.4	1.7	1.9	1.9	1.9	12.0
System % of time in SSA	100%	100%	100%	100%	100%	100%
System % of time in surface monitoring	0.22%	3.85%	8.30%	8.30%	8.30%	1.00%
% time access to earth (O2)	100%	97.6%	95.3%	95.6%	95.9%	69.3%
% time in sun (O1)	100%	95.8%	91.2%	95.4%	93.4%	59.5%

Table 3. SDA performance summary of each architecture against cislunar volume over a lunar day.

SDA	Case 1	Case 2	Case 3	Case 4	Case 5	Case 6
Avg % access (over a month)	76.8 %	67.4 %	64.9 %	64.5 %	72.5 %	48.0 %
Instantaneous (min/max) access	9.3 / 99.8 %	24.1 / 90.8 %	25.5 / 89.6 %	26.6 / 90.1 %	30.0 / 93.9 %	29.2 / 65.9 %
Ramp-up to 50%	0 days	0 days	0 days	0 days	0 days	0 days
Ramp-up to 90%	0 days	5.0 days	5.2 days	4.9 days	4.7 days	5.4 days
Ramp up to 100%	8.8 days	7.8 days	7.7 days	7.6 days	7.5 days	7.9 days
L1 %time in view over month	66.1%	54.6%	53.8%	54.7%	55.5%	38.8%
L1 Gap min/max/mean	3.1/8.4 days	2.06/7.8 days	1.8/7.9 days	2.1/7.9 days	0.5/7.3 days	0.11//8.2 days
L1 avg time in-view	4.5 days	2.5 days	2.1 days	2.5 days	0.7 days	0.07 days
L1 MTTA	1.29 days	1.44 days	1.48 days	1.46 days	1.3 days	1.57 days
L2 %time in view over month	70.7%	60.2%	59.8%	60.7%	57.8%	43.8%
L2 Gap min/max/mean	4.7/7.0 days	3.6/6.1 days	1.8/5.8 days	1.52/5.8 days	0.38/5.5 days	0.09/5.9 days
L2 avg time in-view	9.0 days	6.2 days	2.72 days	2.3days	0.52 days	0.1 days
L2 MTTA	0.91 days	1.07 days	1.04 days	0.99 days	1.02 days	1.07 days

Space Domain Awareness with the Hybrid Sensor

Fig. 11 shows volume access diagrams for each of the selected cases over a lunar day. The plots show percent mono access of the pre-defined cis-lunar volume for cases 1-6, as well as stereo access of the same volume for the tandem cases. The in earth-moon plane sun right ascension is shown as reference to time of the month. From case 1, the tandem N/S L1 NRHO case, we see that there is near constant (>98%) volume access for periods of approximately four days. These effects are likely a product of the individual orbit phasing and can move around or be extended with a tandem phasing optimization. On average, the tandem NRHO architecture can access 76.9% of the pre-defined cis-lunar volume over a lunar day (refer to Table 3). Performance in viewing the L1 and L2 locations from the NRHO configuration is 66.1% and 70.7% for L1 and L2 respectively. Architectures that utilize L1/L2 & N/S NRHOs could be further optimized via permutations, this has been left to future studies or the reader to explore in detail.

Cases 2-4 represent the tandem high eccentricity cases. Access metrics for these cases show an average volume access ranging from 64.5% to 72.5%. The instantaneous max access ranges will vary depending on the time of the month, with favorable access conditions accessing nearly 100% of the volume (~98.5%), and in unfavorable lighting conditions, accessing close to 64% of the volume. The differences between these cases, imply that although small, these apoapsis altitudes of these configurations can be further optimized to increase volume access, or alternatively, can be optimized to spend more time performing lunar monitoring with small penalties to volume access. Access percentage to the L1 location is on-par with the NRHO tandem (case1) and performs slightly better in viewing the L2 location, this is expected. Another key finding, when referring to case 2-4, orbit geometry and periapsis clocking

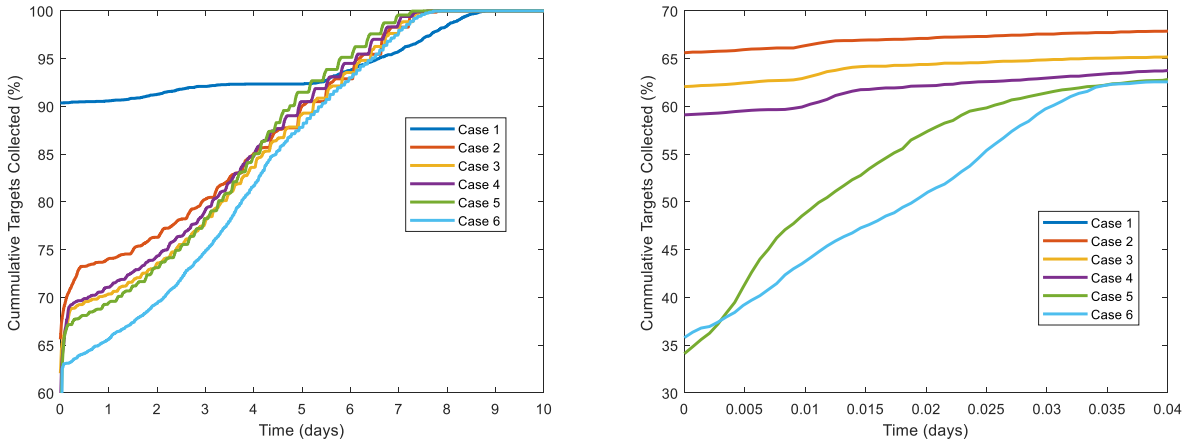

Fig. 10. Cumulative collection performance ramp-up to global access of each sensor architecture.

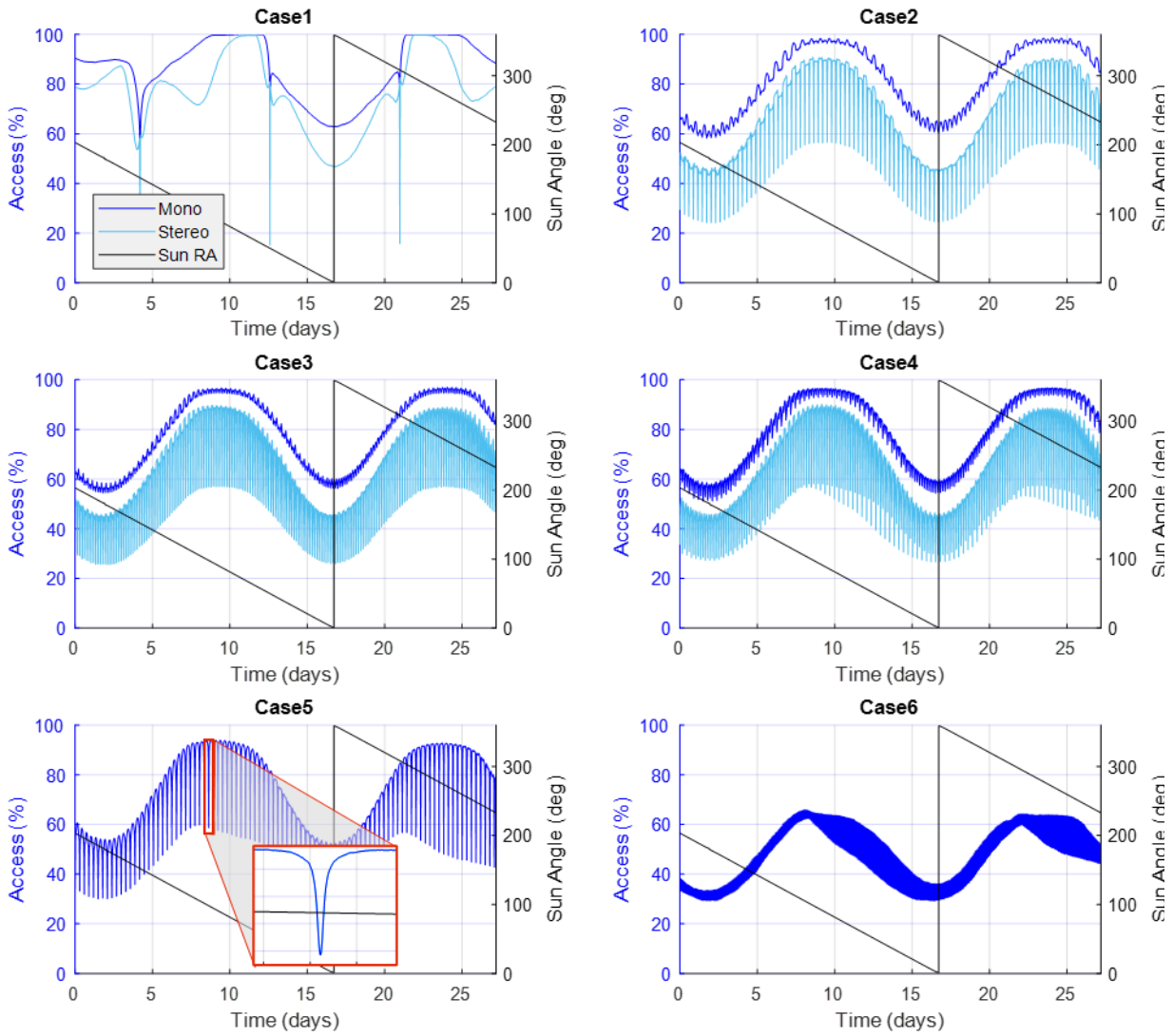

Fig. 11. Instantaneous cislunar volume access per sensor architecture over a lunar day.

seem to have little effect on access performance to cislunar volume. In general, access performance will be dominated by sensor design, and lighting constraints. These findings seem to imply that for orbits this size, the focus of the designer should be on lunar surface access rather than maximizing access to the volume.

Finally, Case 5 and 6 represent the single sensor configurations in a high-eccentric orbit and an LLO at 50km, respectively. Fig. 11 shows access periods for both cases over our simulation period. From Case 5, we can see that, depending on the time of the month, the single sensor architecture can reach access levels ranging from 54% in unfavorable lighting conditions to 93.9% in favorable conditions. The inset in the Case 5 of Fig. 11 shows volume access dropouts to a global minimum of 30.0% resulting from periapsis passes in unfavorable lighting condition. It should be noted that in the lunar surface monitoring configurations, these access periods become unusable. Case 6 assumes space domain awareness at any period of the LLO, performance of this architecture will observe maximum access of 65.9% in favorable lighting conditions and close to 36% in unfavorable conditions.

Fig. 10 represents cumulative collection of each sensor architecture for cases 1-6. Overall, all architectures were able to access 100% of the volume after approximately 8.8 days. The NRHO tandem case benefits from large instantaneous access to the volume, however, it suffers from a slower ramp-up to global access. Alternatively, Case 2-6 can achieve >70% cumulative access metrics within 2 days, with similar ramp ups to global access thereafter. The right side of

Fig. 10 shows the ramp-up of case 5 and case 6 from an initial access of ~35% to access levels above 60% within the first 50 minutes, placing them in family with tandem cases 2-4. These single-sensor architectures represent design options where the mission designer can achieve access to >60% of the volume within 50 minutes, and up to 100% access within 8 days, its likely these metrics are achieved after lighting conditions are favorable to view the volume at the L1 and L2 extremities of our selected cislunar volume. It should be noted that the instantaneous starting access percentage represented in Fig. 10 will be highly dependent on initial orbital geometry and time of the month.

Lunar Surface Monitoring with the Hybrid Sensor

Our assessment of lunar surface access is averaged over a one-year period and is captured in Fig. 12. As expected, Case 1 is the most limited in terms of access to the lunar surface. NRHOs have a consistent access profile over the northern and southern lunar poles, however, given the size of these orbits, the relative velocity and perturbation conditions needed to overcome to use in these applications do not seem practical. From this, we conclude that the NRHOs are challenging from a practical perspective, and thus the value to the Hybrid SDA and lunar surface monitoring activities are limited. Case 2 and 3 represent architectures with periapse placed at the lunar poles, these architectures have a Mean-Time-To-Access (MTTA) rate of once per orbit period at the poles, down to 6 days at latitudes >60° from the equator and no access for latitudes <57° to the equator for Case 2. Case 3 access shows MTTA of <12 days at latitudes >55° from the equator and no access for latitudes <53° to the equator.

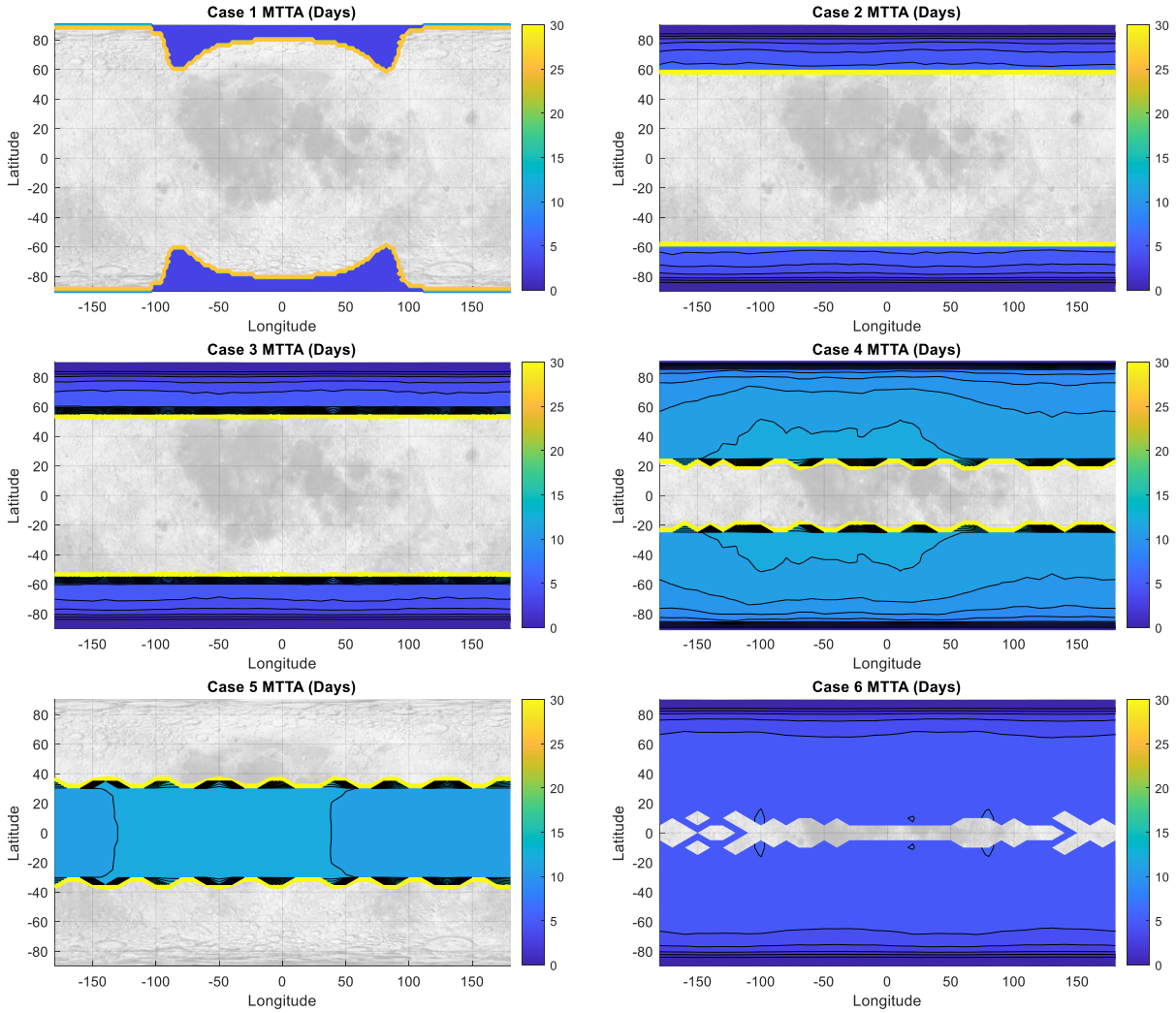

Fig. 12. Global lunar surface access MTTA performance per sensor architecture over year.

The range of latitudes revisited by these orbits is consistent with the surface monitoring true anomaly range defined in Table 2. For case 2, the range of true anomalies accessible to 2m GSD is ±32.6°, while case 3 is ±34.8°. As a result of these surface monitoring true anomaly access ranges as well as the placement of perigee directly over the lunar north/south poles, access to latitudes within 57.4° and 55.1° from the equator, for case 2 and 3 respectively, are nonexistent. Although these cases have limited access to the lower latitudes, revisit rates of the higher latitudes are enhanced due to symmetry about the Eastern/Western lunar hemispheres during these passes. Moving the location of perigee away from the poles allows for access to latitudes closer to the equator to increase, at the cost of Eastern/Western hemisphere "overlap", reducing revisit rates for those regions.

Case 4 of Fig. 12 represents the scenario where we have relocated the location of periapse 35° from the pole; this value coincides with the surface monitoring true anomaly access range defined in Table 2. In this scenario, we expect access to lunar range of latitudes to increase, but the revisit rate of these latitudes to decrease from those seen in case 2 and case 3. As expected, the range of latitudes accessed in case 4 span increases to within 20° from the equator. It's worthwhile noting that these orbits still provide lower MTTAs at the higher latitudes due to more dense overlaps at higher latitudes. At latitudes closer to the equator, we still observe MTTA in the order of 11.7 days. Continuing the trend, a mission designer could continue to move the argument of periapse away from the poles and towards the lunar equator to optimize access latitudes and revisit rates of target latitudes.

Case 5 is a single orbit extreme from Case 2 and 3 in the sense that perigee is placed 90 degrees from the pole. Once again, access latitudes for this case will be related to the surface monitoring true anomaly range defined in Table 2, in this case is ±34.8° in true anomaly, accessing is ±34.8° latitudes. In this case, perigee passes directly over the equator and can access equatorial longitudes with an MTTA of 11.4 days. This configuration can access its highest latitudes with a MTTA of 11.7 days. From here, the analyst can increase/decrease apogee to access larger latitude ranges, as an instance, keeping periapse altitude at 30km and lowering apoapse altitude to ~300km will provide global access to the moon. Alternatively, placing periapse at ±45° latitude and placing apoapse at 5200km altitude will provide full coverage of either the northern or southern hemisphere, depending on selection of periapse placement.

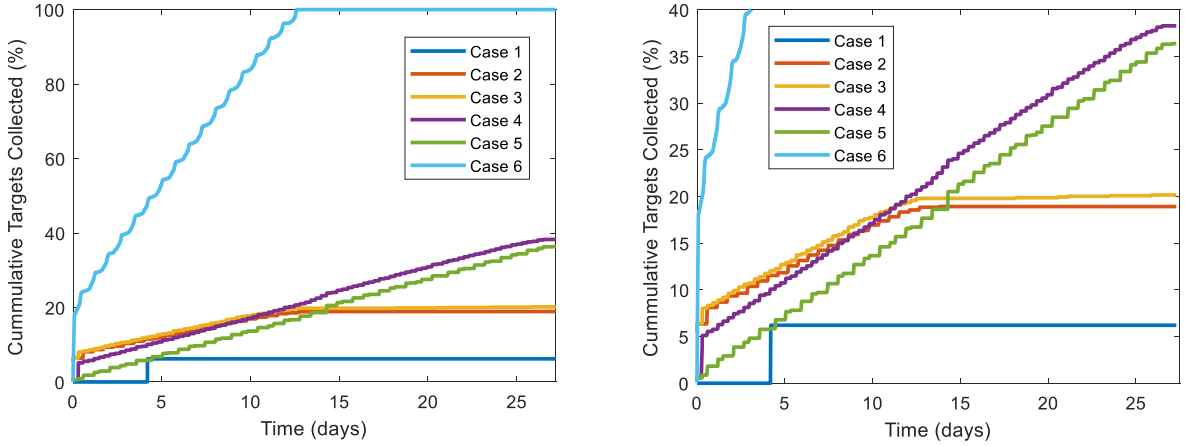

Fig. 13. 1 line plot of 6 cases of % within FOR over one month

Finally, Case 6 is a LLO with an altitude of 50km. This altitude corresponds to an access GSD of just over half a meter. LLOs are interesting since they provide global lunar surface access at high revisit/low MTTA rates while also allowing for a more constrained SDA mission profile. In our analysis, these LLOs can access equatorial latitudes at an MTTA of <6 days, while polar regions can be accessed at an MTTA of once per orbit period. On average, given the orbit period of this circular orbit and 72° half-angle field of regard from nadir, the 50km architecture will have four access passes over an equatorial point over subsequent orbits. This access period is followed by an outage period of roughly 14-days before the opposing node can access the area again. In this configuration, the mission architect can continue to increase/decrease altitude to maintain a desired GSD, maintain a minimum number of accesses per node, while increasing SDA access to the cislunar volume.

6. Conclusion

This paper established a concept capable of lunar surface monitoring and cislunar space domain awareness by operating a single telescope design carefully balanced to reach long ranges in the SDA domain under various lighting conditions and to provide access to various surface locations on the moon. In our tailorable configuration, we select a telescope design with a 1.5° x 6° FOV that can reach sub-2m GSD at altitudes below 150km above the surface of the moon and can detect objects 1m in diameter at distances beyond the L1 and L2 Lagrange points under nominal lighting conditions. The primary benefit of this hybrid sensor design is flexibility in mission utility for lunar surface monitoring and cislunar SDA with a single design. This concept could also be valuable for scientific and strategic purposes, such as measuring the contemporary small-impactor rate by observing small new craters on the lunar surface while gathering surface monitoring in TDI mode or observing impact flashes while observing the dark side of the Moon in framing mode 45.

In our assessment, beyond telescope design, the selection space a mission designer would trade to reach their mission goals as they relate to monitoring of either domain, lunar surface, or deep space was considered. Additionally, the performance characteristics of six selected observing architectures were studied with variations on orbit design parameters to evaluate on the utility of the hybrid concept. As they relate to space domain awareness, our findings indicate the proficiency of this sensor to access the space around the moon and the ability to detect established targets 1m in diameter in cislunar space. As any other SDA sensor, lighting limitations play a role on instantaneous access of cislunar space, however, over a lunar day, the sensor can a large percentage of the relevant volume defined above. The surface monitoring aspect of the design, although limited by a narrow FOV for these types of applications, can support the range of surface dynamics experienced during each periapsis pass for a large range of orbit geometries. The capability to support these imaging conditions, coupled with careful orbit design and the field of regard resulting from these during low altitude access periods provide the potential for frequent monitoring of sites of interest.

The work presented herein does not represent an exhaustive assessment of the telescope trades and their coupling to the orbital design trades that a mission designer may consider to meet their mission needs. Potential future approaches to further leverage the utility of this design entail the definition of over-arching mission requirements for monitoring of each regime, followed by detailed assessment of telescope parameters, orbital parameters, the implications of additional external perturbations to each model (i.e., stray light, spacecraft jitter/smear, as well as more advanced orbit perturbation effects). Other future work includes leveraging repeat ground track approaches for lunar orbiters 10 or other mapping orbits 11 to establish higher refresh/revisit rates for specific surface locations. Initial assessment shows the feasibility of this design is realizable and its value proposition to the mission utility is high, especially as global interest for economic and scientific exploitation of the moon continues to grow.

7. REFERENCES

1. Memorandum of Understanding between the National Aeronautics and Space, Administration and the United States Space Force, NASA.gov, September 21, 2020, accessed October 16, 2020, https://www.nasa.gov/sites/default/files/atoms/files/nasa_ussf_mou_21_sep_20.pdf
2. Brian Banks, Robert D. Smith II, Ronald G. Wagner, Victor M. Aguero, Scott D. Williams, Matthew Duncan, Stijn De Smet, Marc Balducci, *A Sensor-Rich Solution for Lunar/Cislunar Space Domain Awareness*, Advanced Maui Optical and Space Surveillance Technologies Conference (AMOS), September 2020.
3. M. J. Holzinger, C. C. Chow, P. Garretson, *A Primer on Cislunar Space*, 2021, Air Force Research Laboratory, USSF.
4. J. T. S. Cahill and E. J. Speyrer, Assessing the Present-Day Impact Flux to the Lunar Surface Via Impact Flash Monitoring and Its Implications for Sustained Lunar Exploration, *White Paper for the National Academies Planetary Science and Astrobiology Decadal Survey*
5. A. Liakos et al., NELIOTA: Methods, statistics, and results for meteoroids impacting the Moon, *A&A* 633 A112, 2020
6. Mark Beckman and Rivers Lamb, *Stationkeeping for the Lunar Reconnaissance Orbiter (LRO)*, *20th International Symposium on Space Flight Dynamics* 2007.
7. E. Mazarico, G.A. Neumann, D.E. Smith, M.T. Zuber, M.H. Torrence, *Illumination conditions of the lunar polar regions using LOLA topography*, 29 October 2010
8. Emily M. Zimovan, Kathleen C. Howell, and Diane C. Davis, *Near rectilinear halo orbits and their application in cis-lunar space*, IAA-AAS-DyCoSS3-125,
9. Howell, K., *Three-Dimensional, Periodic, 'Halo' Orbits, Celestial Mechanics*, Vol. 32, No. 1, January 1984, pp. 53-71, DOI: https://doi.org/10.1007/BF01358403
10. Ryan P. Russell, Martin Lara, *Repeat Ground Track Lunar Orbits in the Full-Potential Plus Third-Body Problem*, AIAA/AAS Astrodynamics Specialist Conference and Exhibit, 21 - 24 August 2006
11. R V Ramanan, V Adimurthy, *An analysis of near-circular lunar mapping orbits*, J. Earth Syst. Sci. 114, No. 6, December 2005, pp. 619–626